Acid monolayer functionalized iron oxide nanoparticles as catalysts for carbohydrate hydrolysis

Myles Ikenberry, Leidy Peña, Daming Wei, Hongwang Wang, Stefan H. Bossmann, Trenton Wilke, Donghai Wang, Venugopal R. Komreddy, D. Paul Rillema and Keith L. Hohn

Published Version Information

Citation: Ikenberry, M., Pena, L., Wei, D., Wang, H., Bossmann, S. H., Wilke, T., Wang, D., Komreddy, V. R., Rillema, D. P., & Hohn, K. L. (2014). Acid monolayer functionalized iron oxide nanoparticles as catalysts for carbohydrate hydrolysis. Green Chemistry, 16(2), 836-843.

Digital Object Identifier (DOI): 10.1039/c3gc41420e

Publisher's Link: http://pubs.rsc.org/en/content/articlehtml/2014/gc/c3gc41420e

Journal Name

Dynamic Article Links ►

Cite this: DOI: 10.1039/c0xx00000x

www.rsc.org/xxxxxx

ARTICLE TYPE

Acid Monolayer Functionalized Iron Oxide Nanoparticles as Catalysts for Carbohydrate Hydrolysis

Myles Ikenberry[a], Leidy Pena[b], Daming Wei[a], Hongwang Wang[c], Trenton Wilke[a], Donghai Wang[b], Venugopal R. Komreddy[d], D. Paul Rillema[d], Keith L. Hohn[*a]

[a]Department of Chemical Engineering, Kansas State University, Manhattan, KS, USA

[b]Department of Biological and Agricultural Engineering, Kansas State University, Manhattan, KS, USA

[c]Department of Chemistry, Kansas State University, Manhattan, KS, USA

[d]Department of Chemistry, Wichita State University, Wichita, KS 67260-0051206 , USA

Received (in XXX, XXX) Xth XXXXXXXXX 20XX, Accepted Xth XXXXXXXXX 20XX
DOI: 10.1039/b000000x

Abstract

Superparamagnetic iron oxide nanoparticles were functionalized with a quasi-monolayer of 11-sulfoundecanoic acid and 10-phosphono-1-decanesulfonic acid ligands to create separable solid acid catalysts. The ligands are bound through carboxylate or phosphonate bonds to the magnetite core. The ligand-core bonding surface is separated by a hydrocarbon linker from an outer surface with exposed sulfonic acid groups. The more tightly packed monolayer of the phosphonate ligand corresponded to a higher sulfonic acid loading by weight, a reduced agglomeration of particles, a greater tendency to remain suspended in solution in the presence of an external magnetic field, and a higher catalytic activity per sulfonic acid group. The particles were characterized by thermogravimetric analysis (TGA), transmission electron microscopy (TEM), potentiometric titration, diffuse reflectance infrared Fourier transform spectroscopy (DRIFTS), inductively coupled plasma optical emission spectrometry (ICP-OES), and dynamic light scattering (DLS). In sucrose catalysis reactions, the phosphonic-sulfonic nanoparticles (PSNPs) were seen to be incompletely recovered by an external magnetic field, while the carboxylic-sulfonic nanoparticles (CSNPs) showed a trend of increasing activity over the first four recycle runs. The activity of the acid-functionalized nanoparticles was compared to the traditional solid acid catalyst Amberlyst-15 for the hydrolysis of starch in aqueous solution. Catalytic activity for starch hydrolysis was in the order PSNPs > CSNPs > Amberlyst-15. Monolayer acid functionalization of iron oxides presents a novel strategy for the development of recyclable solid acid catalysts.

Introduction

Oil resources are non-renewable, and the expanding economies of the world will require renewable material sources and processing methods if economic development is to be sustainable. Fortunately, the world's annual production of biomass is greater than 170 billion metric tons, and three fourths of that material is carbohydrates, which are thought to be a potential feedstock for a sustainable world chemical industry in the future[1]. One key to this sustainable chemical market is the development of manufacturing processes which inexpensively achieve the necessary material outputs without degrading the environment. Current industrial processes, mainly involving petrochemicals, consume more than 15 million tons of sulfuric acid every year as a non-recyclable catalyst[2]. Replacing sulfuric acid with reusable acid catalysts would be a major achievement towards the goal of sustainable, environmentally-friendly chemical production.

Biofuel production often requires the same acid and base catalysts that are used in other industrial processes, significantly increasing the production costs and environmental impacts of such commodities[3]. For example, the hydrolysis of cellulose into glucose is efficiently catalyzed by sulfuric acid, but the cost associated with waste separation and disposal has prevented an economically efficient large-scale saccharification of cellulosic materials[4]. A heterogeneous catalyst capable of efficiently catalyzing cellulose hydrolysis at mild conditions could reduce the costs associated with waste disposal and enable large-scale

utilization of cellulosic biofuels. Typical solid acid catalysts include sulfonated silicas, zeolites, hetero-polyacids, and ion-exchange resins[2,5]. Stability in water at elevated temperatures remains an important challenge. A recent addition to the family of solid acid catalysts is the material composed of superparamagnetic iron oxide cores, typically surrounded with an organic polymer or silica shell[6–12]. Superparamagnetism provides a facile method of separation which offers these solid acids an advantage over those which require centrifugation or filtration[12]. This paper details a new approach for preparing an acid functionalized superparamagnetic solid acid catalyst: attaching molecules containing acid groups directly to the iron oxide surface in a monolayer.

One way to attach acidic ligands is to choose ligands that have two acids groups: one that can bind to a metal oxide, such as magnetite, and one that will eventually serve as the catalytic site. Portet *et al.*[13] attached di-sulfonic acids to magnetite leaving one sulfonic acid group exposed to solution. However, using a sulfonic acid to bind to magnetite is not optimal due to the sulfonic acid group's weak binding affinity toward the magnetite surface[14,13,15]. The binding strength of typical functional groups to a magnetite surface is given by the order: phosphonic>carboxylic>hydroxyl>sulfonic[16,15]. While phosphonic acids form the strongest bonds to magnetite, they have been associated with substantial decreases in magnetic properties[17], although there is some disagreement[18].

This paper demonstrates that a single ligand can contain a functional group for binding to the nanoparticle surface and an additional catalytically active sulfonic acid group facing outward into solution. This approach takes advantage of differences in the binding affinity of magnetite for different functional groups. In this research, carboxylic/phosphonic acids attach to the magnetic particle and a sulfonic acid group extends away from the particle toward the surrounding solution. The sulfonic acid group is, therefore, available for catalysis. The hydrocarbon chains separating the carboxylic/phosphonic groups from the sulfonic acid group have hydrophobic ligand-ligand interactions which are thought to reduce core-solvent interactions and provide some shielding of the carboxylic/phosphonic acid-magnetite bonds from chemical attack and subsequent ligand dissociation. The structure of the functionalized particles is indicated in Figure 1.

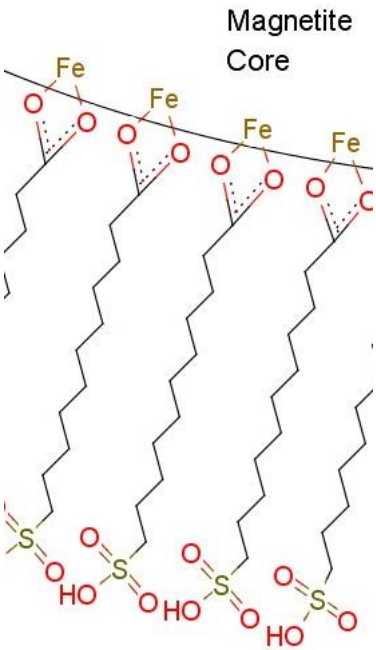

Figure 1: A diagram of the CSNP material composed of a magnetite core, carboxylate-magnetite bonds, an alkane layer, and an outer surface with exposed sulfonic acid groups.

The activity of these acid-functionalized nanoparticles is demonstrated through their use in two acid-catalyzed reactions: hydrolysis of sucrose to glucose and fructose, and hydrolysis of starch to glucose[5]. The activity of magnetite nanoparticles bound to carboxylic and phosphonic acid ligands are compared with that of a common solid acid catalyst, Amberlyst-15. Furthermore, the reusability of the acid-functionalized nanoparticles is demonstrated by following their activity over multiple uses.

Experimental

Synthesis of 11-sulfoundecanoic acid and 10-phosphono-1-decanesulfonic acid

11-sulfoundecanoic acid was synthesized from 11-bromoundecanoic acid and sodium sulfite according to a previously published procedure[19]. The 11-bromoundecanoic acid was combined with sodium sulfite in a 10:1 ratio and the reagents were heated at 50°C for 1 hour, 70°C for 2 hours, 80°C for 6 hours, then 90°C for 3 hours. The product was separated from solution by first lowering the pH to 5 with HCl and filtering under vacuum at 50°C, then placing the filtrate in an oven for one week at 80°C to fully oxidize the sodium sulfite impurity salt into sodium sulfate. The baked precipitate was then placed in concentrated hydrochloric acid solution and centrifuged to precipitate the purified ligand and leave the remaining sodium sulfate and sodium bromide in the acid solution. Full oxidation of the sodium sulfite is necessary to ensure that hydrochloric acid addition does not produce dangerous sulfur trioxide gas. The centrifugation was repeated three times. Then, the precipitated ligand was vacuum dried overnight at room temperature to remove excess HCl.

10-phosphono-1-sulfonodecanic acid was synthesized as

illustrated in Figure 2†. Briefly, the intermediate compound 1,10-dibromodecane was synthesized from 1,10-butanediol by heating in hydrobromic acid at 100°C for 48 hours. After the reaction, it was extracted with chloroform, washed with brine, stirred over sodium bicarbonate, then filtered and passed through Na_2SO_4. The obtained compound was purified by column chromatography on silica gel, yielding 1,10-dibromodecane as white crystals. The 1,10-dibromodecane was heated to 155°C in an oil bath under argon, then triethylphosphite was added dropwise over 8 hr. Cooling to room temperature produced a white precipitate, which was separated by filtration and purified by flash column chromatography. Diethyl(10-bromodecyl)phosphonate was then heated in a saturated solution of Na_2SO_3 at reflux for one hour then at 120°C until the solvent evaporated. The residue was then slurred with CH_3OH under reflux and the hot solution was filtered. The filtrated was then evaporated and the residue acidified with hydrobromic acid and refluxed for 48 hours. Evaporation of the acid under reduced pressure produced a pale-black powder.

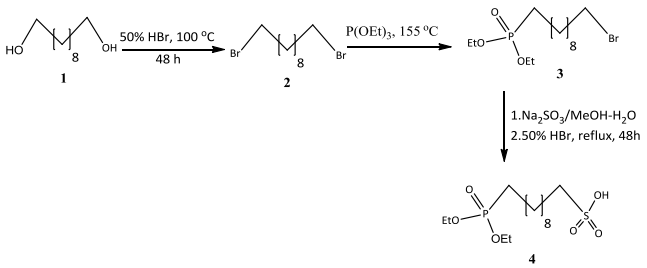

Figure 2. Sequence of steps[20–22] used to prepare diethyl(sulfonyldecyl)phosphate (4).

Nanoparticle synthesis and functionalization

Iron oxide nanoparticle cores were prepared using a modification of Massart's precipitation method[23,24]. Iron (II) chloride and iron (III) chloride in a 1:2 molar ratio were precipitated with ammonium hydroxide at 80°C, heated for 30 minutes, and then sonicated for 20 minutes. 1g of the synthesized di-acid ligand was added to 1g of the sonicated particles, and the mixture was sonicated for 10 minutes, then heated to 95°C for 30 minutes. The 95°C particles were sonicated for an additional 10 minutes, then returned to the oil bath. After 24 hours of stirring at 95°C, the solution was allowed to return to room temperature under constant stirring for 12 hours, then reheated to 95°C and stirred for another 24 hours, and then again allowed to return to room temperature.

Washing at room temperature was achieved by repeatedly mixing the nanoparticles with water and magnetically extracting the particles from solution. The washwater was initially clear and then on subsequent washes became darker as the particles became increasingly difficult to separate from solution. As the concentration of unbound ligand in the supernatant decreased during the washing process, the supernatant did not become clear in the presence of the neodymium supermagnet (with field strength of 3661 Gauss).

After 5 washes, the PSNP supernatant, which was not clear, was measured by DLS as 50 nm agglomerates. The separable particles, when re-suspended, also measured as 50 nm agglomerates. Increasing the concentration of re-suspended particles did not increase the measured size of particle agglomerates, possibly indicating that individual particles were present in solution, instead of agglomerates. The combined supernatant/particle mixture was then subjected to centrifugation (10,000 rpm for 1 hour at 4°C). The supernatant was discarded, and the centrifuged solid was then re-suspended in DI water and vigorously agitated for 5 minutes. The centrifugation-washing was repeated twice more.

Washing the CSNP particles five times gave a suspension which was not fully separable by the supermagnet. After a few days of sitting at room temperature, the particles had agglomerated to the stir bar magnet, leaving a clear supernatant. They were washed another 5 times by supermagnetic particle separation to further remove unbound ligand. The PSNPs and CSNPs were not dried after washing. Instead, a washed catalyst solution of known catalyst dry weight concentration was added to DI water to obtain reaction solutions.

Catalyst Characterization

To calculate the acid loading of all catalysts, 0.05 grams (dry wt.) of wet catalyst solution were titrated with 0.01 M NaOH solution. For TGA, the samples were analyzed in a PerkinElmer Pyris1 TGA (Norwalk, CT). Approximately 5 mg of each sample was heated under a nitrogen atmosphere from 50°C to 600°C at a rate of 10°C/min. Transmission electron microscope (TEM) images were used to estimate the size distribution of the nanoparticles. A model CM100 TEM (FEI Company, Hillsboro, OR), equipped with an AMT digital image capturing system, was operated at 100 kV. The images were taken of dispersed particles deposited from aqueous solutions by contacting a drop of liquid with Formvar/ carbon-coated, 200-mesh copper grids (Electron Microscopy Sciences, Fort Washington, PA) for 30 seconds at room temperature. Nanoparticle mean diameters were calculated from the TEM images using the software ImageJ, available from the National Institute of Health. Particle agglomerate data was taken on a ZetaPALS Zeta Potential Analyzer (Brookhaven Instruments Corporation) with hydrodynamic light scattering.

XRD analysis was conducted using a Rigaku MiniFlex II desktop x-ray diffractometer, using a fixed time scanning method with a 0.01° step size and 6 seconds counting time at each step. The phase composition of the nanoparticles was estimated using the relative intensity ratio method within Rigaku's PDXL software. Crystallite sizes were calculated using the Scherrer formula. The crystallite size is used as an approximation of the magnetite particle size, as described by other investigators[23]. Diffuse reflectance infrared Fourier transform spectroscopy (DRIFTS) was conducted on a Thermo Nicolet NEXUS 870 spectrometer with a ZnSe window, operated by the software program OMNIC. Samples were dried at 50°C for 48 hours. KBr was used for a background scan, then immediately added to a spec of dried sample, ground up by mortar and pestle, and returned to the cell for analysis. ICP-OES was conducted with a Varian 720-ES ICP Optical Emission Spectrometer. Standards were prepared from stock solutions of Fe, S, and P, and used for calibration. The lines selected for each element were Fe 259.94 nm, P 178.29 nm, S 181.97 nm.

Catalytic Activity Measurement

Sucrose hydrolysis was conducted by 80 °C for 6 hours in a sealed vial with magnetic stirring, using 0.05g of catalyst and 0.1g of sucrose in 5g of water. Reaction temperature was controlled using an oil bath held at constant temperature, with reactor temperature periodically checked with a temperature probe. After the completion of each run, the catalyst was separated either by supermagnet or by centrifugation. Fresh sucrose and 5g of water were placed in the reaction vessel, which was returned to the oil bath for the next round of reaction. To test the reproducibility of the sucrose experiments, three runs were conducted on three different CSNP samples. Control runs with no catalyst present showed no conversion.

For starch hydrolysis, 0.002g (dry wt.) of PSNPs, 0.017g (dry wt.) of CSNPs, or 0.0006g Amberlyst-15 were added with 0.09g starch and 5g of water so as to yield an acid site:starch:water mol ratio of 1:200: 100,000 for Amberlyst-15 and 1:400:200,000 for the CSNPs and PSNPs. In a sealed glass tube with magnetic stirring at 300 rpm, the mixtures were placed in an oil bath at 130°C for 24 hours. CSNPs and PSNPs were both separated by centrifugation at 10,000 rpm for 1 hour at 4°C. The centrifuged catalyst was combined with 5g of water and 0.09g of starch and returned to the reaction vessel for the next run. To estimate the variability of the experimental setup, 3 runs with fresh Amberlyst-15 were run, and a standard deviation of 3.7% was found. Control runs with no catalyst present showed no conversion.

Sugar analysis was conducted using an HPLC RCM-Ca+2 monosaccharide column (300 × 7.8 mm; Phenomenex, Torrance, CA) with a refractive index detector. The HPLC was calibrated to external standards for sucrose, glucose, fructose, and maltose, using 80°C deionized water at a flow rate of 0.6 mL/minute. During HPLC analysis, samples were alternated with known standards to ensure accuracy of the measurements.

Results and Discussion

Catalyst Characterization

DRIFTS spectra of the ligands, CSNPs, and NaOH neutralized PSNPs are shown in Figure 3. RSO_3^- and RPO_3^- groups appeared around 1050 and 1180 cm^{-1} due to asymmetric and symmetric vibrations, respectively[17]. Both NPs have a peak at 1467 cm^{-1} corresponding to the CH_2 scissoring bend[17]. CSNPs, PSNPs, and the 11-sulfoundecanoic acid show a peak around 1556 cm^{-1} which may be due to sodium sulfonate. The sodium in the CSNPs may originate from sodium impurity in the synthesized 11-sulfoundecanoic acid, while sodium in the PSNPs comes from the addition of NaOH to a limited supply of catalyst. For CSNPs, an overlapping peak at 1544 cm^{-1} is due to asymmetric COO^- stretching. The CSNP peak at 1626 cm^{-1} corresponds to COO^- symmetric stretch. The distance between the asymmetric and symmetric COO^- peaks being less than 110 cm^{-1} is an indication of chelating bidentate attachment[25] or chelating mononuclear attachment[26]. When carboxylic acid COOH groups are uncoordinated, a peak around 1710 cm^{-1} is present[27,28]. The peak for free carboxylic acid is observed in the 11-sulfoundecanoic acid. The lack of this peak in the spectrum of the CSNPs indicates a lack of free COOH. The alkane chain vibrations appear at 2852 and 2921 cm^{-1} for PSNPs, with CSNPs showing corresponding peaks at 2850 and 2918 cm^{-1}. The NP alkane vibrations are at lower wavenumbers than the corresponding free acids, indicating confinement and ordered packing on the particle surfaces[29]. The ligands and NPs all had a broad OH vibration band between 3200 and 3600 cm^{-1} (not shown).

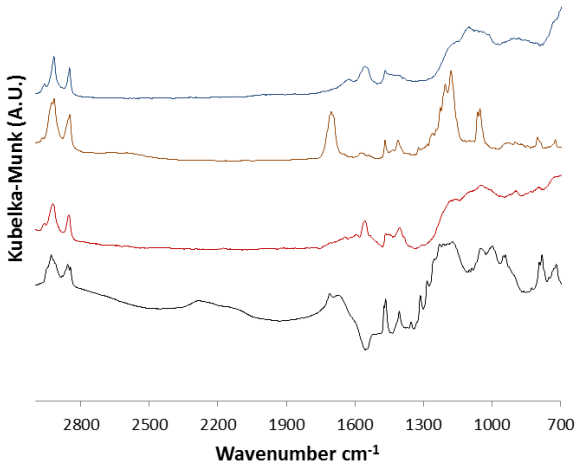

Figure 3. DRIFTS spectra of the a) CSNPs b) 11-sulfoundecanoic acid c) NaOH neutralized PSNPs d) 10-phosphono-1-decanesulfonic acid

TGA results for both PSNPs and CSNPs are shown in Figure 4. By 200°C, the CSNPs had lost about 1% of its weight, and the PSNPs had lost about 2%. Some of the weight loss may be due to water. For CSNPs, the total weight loss was 5.6% by weight. If this entire weight loss is ascribed to ligand desorption and decomposition, it corresponds to a sulfur content of 0.69%, or 0.2 mmol/g sulfur in the CSNPs. That is higher than the acid loading of 0.08 mmol H^+ per gram as determined by titration of the CSNPs. For the PSNPs, the weight loss during TGA was 18.7%, and the titrated acid loading was 0.65 mmol H^+ per gram. The ligand loading calculated from titration of the PSNPs is roughly in agreement with what is indicated from TGA. During TGA of functionalized iron oxide nanoparticles, it is thought that some carbon remains on the particle surface due to incomplete decomposition of the organic ligands, and the formation of graphitic species[26].

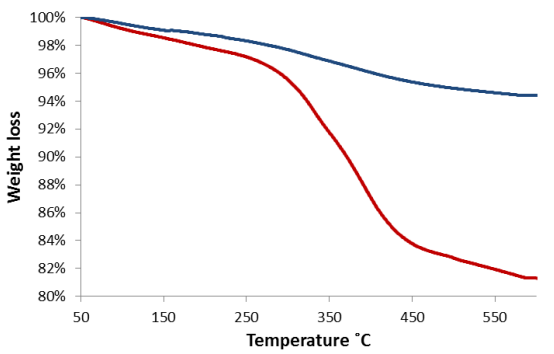

Figure 4. TGA graph of catalyst weight % vs. the temperature (°C). The total weight loss is a) 5.6% for the CSNPs and b) 18.7% for the PSNPs

We can further understand how the acid-containing ligands pack on the surface by using particle surface area to estimate the packing density. The packing density of the ligand layer on the particle surface is important for many reasons. A more tightly packed full monolayer will obviously result in a higher acid site density on the outer surface and a higher ligand loading by weight. Additionally, a tightly packed ligand layer may be more likely to protect the magnetite layer from oxidation and a corresponding reduction in magnetic properties. Prevention of magnetite degradation, along with the loss of acid groups, is a primary concern in the design of acid functionalized iron oxide nanoparticles. The average particle diameter for the bare particles was estimated at 10.5 nm from the Scherrer equation. For phosphonate ligand heads taking up 0.24 nm2, this corresponds to a monolayer loading of 0.76 mmol/g, which is slightly higher than the phosphonic acid loading of 0.65 mmol/g indicated from titration. Some researchers believe that phosphonates bind in a tridentate fashion[30] but others suggest only bidentate binding[17].

X-ray diffraction results (Figure 5) indicate significant differences in the iron oxide phase compositions of CSNPs and PSNPs. Magnetite and maghemite are present in both CSNPs and PSNPs, with PSNPs showing substantially higher maghemite content. Additionally, the goethite phase of iron oxide is present in the PSNPs but not in the CSNPs or bare particles, as demonstrated by the XRD peaks at 21.18°, 33.20°, 39.93°, 41.16°, 50.65°, 53.16°, 58.98°, and 61.29°, which are marked on Figure 5. Carboxylic acids and other ligands are thought to rearrange the surfaces of metal oxide nanoparticles[31,32]. This does not necessarily mean a degradation of magnetic properties[33,18]. PSNP and CSNP diameters are estimated as 10.9 and 11.5 nm, respectively.

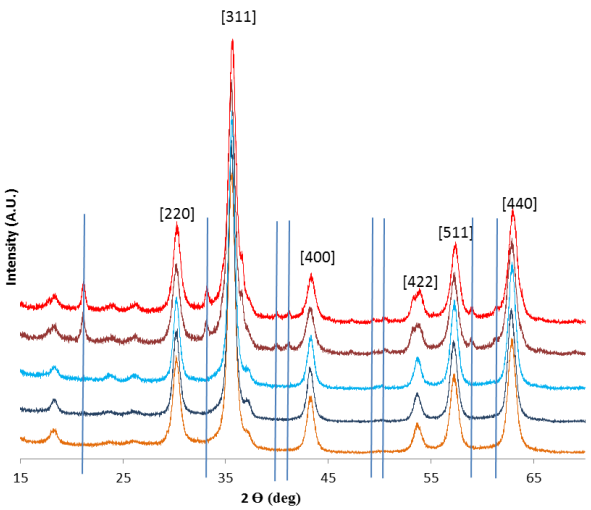

Figure 5. XRD for a) PSNPs after 18 hours of starch hydrolysis at 130°C b) PSNPs as synthesized c) CSNPs after 18 hrs starch hydrolysis at 130°C d) CSNPs as synthesized e) bare particles. Lines denote goethite peaks.

Catalysis of starch and sucrose hydrolysis

The conversion of sucrose for three different CSNP samples over multiple consecutive runs is shown in Figure 6. The CSNP catalytic activity increases through the first 4 runs, using centrifugation for separation of particles between runs. After the 4th cycle, the catalyst was refrigerated and stored for one week before being used again in recycle reactions 5-9, with magnetic particle separation. Sucrose conversion for trials 5-9 is relatively constant at ~60%. As seen in Figure 6, the increasing activity over the first four recycles was noted for three different CSNP samples, providing strong evidence that this was a real trend.

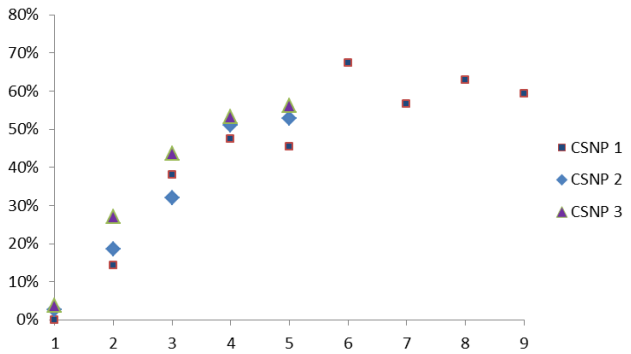

Figure 6. CSNP sucrose activity at 80 °C using 0.05 g catalyst, 0.1 g sucrose, and 5g water.

An increase in catalytic activity during recycle runs is unusual. One possible explanation for this trend is that some ammonium may have remained coordinated to the sulfonate groups after synthesis and become detached during the catalytic runs. Another possibility is that changes in agglomerate size may impact the catalytic activity. In aqueous solutions of functionalized iron oxide nanoparticles, agglomeration often decreases at higher temperatures[34].

The de-agglomeration of CSNPs was observed in TEM images, as shown in Figure 7. On the left, the agglomeration of primary particles leaves only a single non-agglomerated particle to be seen in the TEM image. In the image on the right, 6 hours of sucrose hydrolysis at 80°C has caused the agglomeration to decrease significantly.

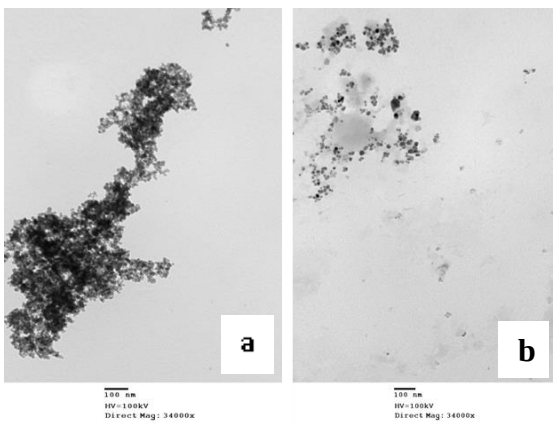

Figure 7. TEM images of CSNPs deposited a) at room temperature in pure water b) from an aqueous 80°C sucrose solution after a 6 hour reaction.

The CSNP de-agglomeration during sucrose reactions was also

measured with DLS, by adding drops of hot reaction solution to a heated cell containing 70°C sucrose solution. These conditions were chosen to minimize agglomerate changes during the DLS measurement of the reaction mixture. DLS measurements of the CSNPs taken at the beginning and end of a 6-hour sucrose reaction indicated that the initial effective agglomerate size of 3000-4000 nm was reduced to less than 1000 nm by the end of a reaction cycle. The necessary dilution for DLS measurement may have caused some de-agglomeration.

The PSNP catalytic activity for sucrose hydrolysis is shown in Figure 8 for 17 consecutive 6-hour runs. Catalyst separation was achieved by using an external magnetic field in runs 1-13 and by centrifugation in runs 14-17. As seen in Figure 8, conversion is between 40 and 50% for the first four runs, but then shows a decrease to less than 20% by the 13th run. This decrease is due to the loss of magnetic particles in the recycling process. PSNPs are quite stable in solution, so a certain amount is not able to be extracted even by the high powered magnet. Figure 9 is a photograph of the supernatants following reaction and removal of PSNPs with the magnet. The darker colors observed are an indication that some PSNPs remain in the supernatant.

To understand whether the loss in activity noted over 13 runs was entirely due to the loss of PSNP particles or whether some other deactivation was occurring, the supernatants collected in the first 13 runs were centrifuged to recover more of the suspended catalyst for reuse. The recovered catalyst was combined with the catalyst that had been magnetically recovered successfully. The recombined catalyst was then used in further reactions. As seen in Figure 8, PSNP conversion returned to over 40% for runs 15-17, indicating that the catalyst had not been deactivated.

At this time, it is not possible to eliminate the detachment of ligands as partially responsible for the lower conversion noted for recycle runs 5-13. The phosphonate-magnetite bond is expected to be quite strong, so we do not expect ligand loss from the monolayer. For runs 15-17, centrifugation was used to recycle the PSNPs. A conversion above 40% for all recycle runs indicates that centrifugation is superior to magnetic separation when recycling the PSNPs. This might be an indication that the magnetic character of the magnetite core is damaged by the attachment of the phosphonate ligands. This is supported by the XRD data that shows the presence of a new iron phase goethite (α-FeOOH) in addition to substantially increased maghemite (Fe_2O_3), after phosphonate ligand attachment.

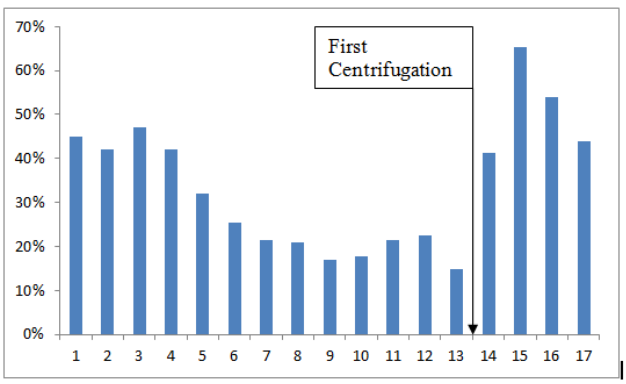

Figure 8. PSNP sucrose activity for reactions 1-17 at 80 °C using 0.05 g catalyst, 0.1 g sucrose, and 5g water.

Figure 9. 6-hour sucrose reaction supernatants with PSNPs remaining in suspension in the presence of a powerful magnetic field.

The PSNPs are not easily separated from solution. Centrifugation is more effective, but neither centrifugation nor magnetic field is able to achieve complete separation of particles from supernatants. This may be due to a combination of factors such as increased hydrophilic character from the increased number of sulfonic acid groups, increased hydrophilic character due to the more highly packed and less exposed lipid layer, decreased agglomerate sizes resulting in smaller effective magnetic force per particle, and possibly decreased particle magnetic strength. PSNPs titrated to a pH of 7 gave distinct TEM images: individual particles averaged 5.2 nm, and agglomerates of larger particles averaged 12.9 nm.

ICP was used to gain some information about the atomic composition of the supernatants after catalyst removal. These data (shown in Table 1) indicate a ratio of iron to phosphorus that is around 2:1 for the combined supernatants of runs 1-13, and around 4:1 for the individual supernatants of runs 14-16. For a monolayer of 10-phosphono-1-decanesulfonic acid calculated using a ligand head area of 0.24 nm^2, the Fe:P ratio varies from 15 to 58, for 5nm and 20 nm particles, respectively.

Run	Fe(ppm)	P (ppm)	S (ppm)
1 to 13	20	9	9
14	19	5	5
15	47	10	12
16	26	6	8

Table 1. ICP data for the inseparable catalyst remaining in solution after 6 hour sucrose runs.

The incomplete separation of particles from solution, combined with the correlation between ligand loading and particle size, makes the interpretation of ICP data difficult. A shift in Fe:P ratio can reflect not only a change in the relative amounts of free ligand and particles, but also in the diameter distribution of particles which remain suspended. The ICP data seems to indicate that some excess ligand is lost, although this does not result in a decrease in catalytic activity after the initial 4 runs. The trend of catalytic activity increase seen for the CSNPs may be present in the PSNPs as well, but counteracted by the loss of excess ligand. The issue of incomplete catalyst recovery in the PSNP sucrose runs may complicate an accurate assessment of the catalytic activity.

To compare the activity of CSNPs vs. PSNPs, the starch hydrolysis data may be more useful since centrifugation is used to maximize catalyst recovery after each reaction. Acid site turnover frequency (moles of glucose formed per mole of acid per hour) for PSNPs, CSNPs, and Amberlyst-15 is shown in Figure 10. The PSNPs show the highest activity for starch hydrolysis, surpassing the CSNPs and Amberlyst-15. The increased ligand loading achieved using the phosphonic acid attachment apparently also results in an outer surface whose acid sites are

individually more active. Unfortunately, there is a trade-off between the benefits and downsides of a more highly hydrophilic outer surface. Even in centrifugation, the PSNPs leave the supernatant visibly darkened with the presence of particles. The presence of particles was again confirmed with ICP data showing the presence of iron, sulfur, and phosphorus in the post-centrifugation supernatants. The downside of decreased catalytic recovery is a significant one. If larger particles are more easily recovered, the lower acid loading by weight may be a reasonable trade-off. Further research should investigate monodisperse particles for activity and recycle potential.

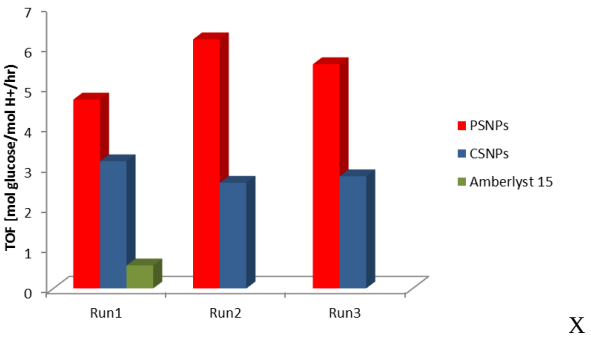

X

Figure 10. TOF [mol glucose (mol H^+) $^{-1}$ hr $^{-1}$] for three runs of 24 hour starch hydrolysis at 130°C

For both the CSNPs and PSNPs, the activity seen is an average over particles of significantly different radii and surface curvature. Beyond the immediate geometrical trends, the smaller particles are likely to behave differently from larger ones. For example, smaller iron oxide nanoparticles have been seen to form more tightly packed monolayers than larger particles[25]. This may compound the effect of increased surface area and further increase the weight loading of ligand on smaller particles. However, since phosphonic acids bind more strongly than carboxylic acids to magnetite, the monolayer density as a function of particle size may be less pronounced in PSNPs than in CSNPs. Another interesting effect of the nanoparticle curvature is the tendency to push acid groups closer together at larger particle sizes[35]. It is unclear whether this effect increases acid site activity[36] or decreases it[35].

Conclusions

Monolayer acid funtionalized iron oxide nanoparticles have the potential for facile recyclability, high acid loading, high acid site catalytic activity, and stability in aqueous solutions at elevated temperatures. CSNPs have been shown to possess an interesting trend of increasing catalytic activity through initial catalytic reactions, likely because of deagglomeration of particles at the high temperatures of reaction. PSNPs have higher acid loading and acid site activity compared to CSNPs, but lower recyclability. The analysis of PSNP data is complicated by incomplete catalyst recovery and variations in ligand loading between various particle sizes. Future work should explore functionalizations of monodisperse iron oxide particles to evaluate the optimal particle size which results from the tradeoff between recyclability and acid site loading/activity.

Notes and references

[a] *1016 Durland Hall, Manhattan, KS 66506-5102, USA, Fax: 785-532-7372; Tel: 785-532-4315 E-mail: hohn@ksu.edu*

† Electronic Supplementary Information (ESI) available: complete reaction details for 10-phosphono-1-sulfonodecanic acid. See DOI: 10.1039/b000000x/

1. A. Corma, S. Iborra, and A. Velty, *Chemical reviews*, 2007, **107**, 2411–502.
2. M. Hara, T. Yoshida, A. Takagaki, T. Takata, J. N. Kondo, S. Hayashi, and K. Domen, *Angewandte Chemie (International ed. in English)*, 2004, **43**, 2955–8.
3. F. Carvalheiro, L. C. Duarte, and F. M. Gírio, *Journal of Scientific & Industrial Research*, 2008, **67**, 849–864.
4. S. Van de Vyver, L. Peng, J. Geboers, H. Schepers, F. de Clippel, C. J. Gommes, B. Goderis, P. a. Jacobs, and B. F. Sels, *Green Chemistry*, 2010, **12**, 1560.
5. P. L. Dhepe, M. Ohashi, S. Inagaki, M. Ichikawa, and A. Fukuoka, *Catalysis Letters*, 2005, **102**, 163–169.
6. N. T. S. Phan and C. W. Jones, *Journal of Molecular Catalysis A: Chemical*, 2006, **253**, 123–131.
7. C. Gill, B. Price, and C. Jones, *Journal of Catalysis*, 2007, **251**, 145–152.
8. J. Lee, Y. Lee, J. K. Youn, H. Bin Na, T. Yu, H. Kim, S.-M. Lee, Y.-M. Koo, J. H. Kwak, H. G. Park, H. N. Chang, M. Hwang, J.-G. Park, J. Kim, and T. Hyeon, *Small (Weinheim an der Bergstrasse, Germany)*, 2008, **4**, 143–52.
9. L. Peña, M. Ikenberry, B. Ware, K. L. Hohn, D. Boyle, X. S. Sun, and D. Wang, *Biotechnology and Bioprocess Engineering*, 2011, **16**, 1214–1222.
10. M. Feyen, C. Weidenthaler, F. Schüth, and A.-H. Lu, *Chemistry of Materials*, 2010, **22**, 2955–2961.
11. D. Lai, L. Deng, J. Li, B. Liao, Q. Guo, and Y. Fu, *ChemSusChem*, 2011, **4**, 55–8.
12. D. Lai, L. Deng, Q. Guo, and Y. Fu, *Energy & Environmental Science*, 2011, **4**, 3552.
13. D. Portet, B. Denizot, E. Rump, J.-J. Lejeune, and P. Jallet, *Journal of Colloid and Interface Science*, 2001, **238**, 37–42.
14. L. Vekasa, D. Bica, and M. Avdeev, *China Particuology*, 2007, **5**, 43–49.
15. R. Cornell and U. Schwertmann, *The iron oxides: Structure, properties, reactions, occurrences, and uses*, Wiley-VCH, 2nd edn., 2003.
16. Y. Sahoo, H. Pizem, T. Fried, D. Golodnitsky, L. Burstein, C. N. Sukenik, and G. Markovich, *Langmuir : the ACS journal of surfaces and colloids*, 2001, **17**, 7907–7911.
17. C. Yee, G. Kataby, A. Ulman, T. Prozorov, H. White, A. King, M. Rafailovich, J. Sokolov, and A. Gedanken, *Langmuir : the ACS journal of surfaces and colloids*, 1999, **15**, 7111–7115.
18. T. J. Daou, J. M. Grenèche, G. Pourroy, S. Buathong, a. Derory, C. Ulhaq-Bouillet, B. Donnio, D. Guillon, and S. Begin-Colin, *Chemistry of Materials*, 2008, **20**, 5869–5875.
19. J. Cui, D. Cao, and C. Xu, *Chinese Journal of Synthetic Chemistry*, 2006, **14**, 529–531.
20. S. De, V. K. Aswal, and S. Ramakrishnan, *Langmuir : the ACS journal of surfaces and colloids*, 2010, **26**, 17882–9.
21. X. Wang and M. Lieberman, *Langmuir : the ACS journal of surfaces and colloids*, 2003, **19**, 7346–7353.
22. D. Taffa, M. Kathiresan, and L. Walder, *Langmuir : the ACS journal of surfaces and colloids*, 2009, **25**, 5371–9.
23. Y. Sahoo, A. Goodarzi, M. T. Swihart, T. Y. Ohulchanskyy, N. Kaur, E. P. Furlani, and P. N. Prasad, *The journal of physical chemistry. B*, 2005, **109**, 3879–85.
24. R. Massart, *IEEE Transactions on Magnetics*, 1981, **17**, 1247–1248.
25. L. Zhang, R. He, and H.-C. Gu, *Applied Surface Science*, 2006, **253**, 2611–2617.
26. P. Roonasi and A. Holmgren, *Applied Surface Science*, 2009, **255**, 5891–5895.

27. K. V. P. M. Shafi, A. Ulman, X. Yan, N. Yang, and C. Estourne, *Langmuir : the ACS journal of surfaces and colloids*, 2001, **17**, 5093–5097.
28. K. Yang, H. Peng, Y. Wen, and N. Li, *Applied Surface Science*, 2010, **256**, 3093–3097.
29. K. Nakamoto, *Infrared and Raman Spectra of Inorganic and Coordination Compounds*, John Wiley & Sons, New York, 1997.
30. S. Mohapatra and P. Pramanik, *Colloids and Surfaces A: Physicochemical and Engineering Aspects*, 2009, **339**, 35–42.
31. T. Rajh, L. X. Chen, K. Lukas, T. Liu, M. C. Thurnauer, and D. M. Tiede, *Journal of Physical Chemistry B*, 2002, **106**, 10543–10552.
32. S. Laurent, D. Forge, M. Port, A. Roch, C. Robic, L. Vander Elst, and R. N. Muller, *Chemical reviews*, 2008, **108**, 2064–110.
33. H. Duan, M. Kuang, X. Wang, Y. A. Wang, H. Mao, and S. Nie, *Journal of Physical Chemistry C*, 2008, **112**, 8127–8131.
34. H. Kikura, J. Matsushita, M. Matsuzaki, Y. Kobayashi, and M. Aritomi, *Science and Technology of Advanced Materials*, 2004, **5**, 703–707.
35. D. Wang, R. J. Nap, I. Lagzi, B. Kowalczyk, S. Han, B. a Grzybowski, and I. Szleifer, *Journal of the American Chemical Society*, 2011, **133**, 2192–7.
36. I. Mbaraka and B. Shanks, *Journal of Catalysis*, 2006, **244**, 78–85.

1 A. Name, B. Name and C. Name, *Journal Title*, 2000, **35**, 3523; A. Name, B. Name and C. Name, *Journal Title*, 2000, **35**, 3523.